The Astrophysical Journal Letters, 724:L194–L198, 2010 December 1 doi:10.1088/2041-8205/724/2/L194

PERIODIC SPECTRAL LINE ASYMMETRIES IN SOLAR CORONAL STRUCTURES FROM SLOW MAGNETOACOUSTIC WAVES

E. Verwichte[1], M. Marsh[2], C. Foullon[1], T. Van Doorsselaere[1,4], I. De Moortel[3], A. W. Hood[3], and V. M. Nakariakov[1]
[1] Centre for Fusion, Space and Astrophysics, Department of Physics, University of Warwick, Coventry CV4 7AL, UK; Erwin.Verwichte@warwick.ac.uk
[2] Jeremiah Horrocks Institute for Astrophysics & Supercomputing, University of Central Lancashire, Preston PR1 2HE, UK
[3] School of Mathematics and Statistics, University of St Andrews, St Andrews KY16 9SS, UK
Received 2010 August 11; accepted 2010 September 16; published 2010 November 10

ABSTRACT

Recent spectral observations of upward moving quasi-periodic intensity perturbations in solar coronal structures have shown evidence of periodic line asymmetries near their footpoints. These observations challenge the established interpretation of the intensity perturbations in terms of propagating slow magnetoacoustic waves. We show that slow waves inherently have a bias toward enhancement of emission in the blue wing of the emission line due to in-phase behavior of velocity and density perturbations. We demonstrate that slow waves cause line asymmetries when the emission line is averaged over an oscillation period or when a quasi-static plasma component in the line of sight is included. Therefore, we conclude that slow magnetoacoustic waves remain a valid explanation for the observed quasi-periodic intensity perturbations.

Key words: line: formation – magnetohydrodynamics (MHD) – Sun: corona – Sun: oscillations

Online-only material: color figure

1. INTRODUCTION

Quasi-periodic intensity perturbations propagating upward along coronal structures are known to exist in coronal plumes (Ofman et al. 1997; DeForest & Gurman 1998) and loops (Berghmans & Clette 1999; Schrijver et al. 1999). These phenomena have been studied extensively using extreme ultraviolet (EUV) images (e.g., De Moortel et al. 2000, 2002; Robbrecht et al. 2001; King et al. 2003; Marsh et al. 2003, 2009; McEwan et al. 2006) and exhibit the following observational signatures (see recent review by De Moortel 2009): intensity amplitudes of 1%–15%, propagation speeds between 45 and 205 km s^{-1}, and periodicities in the range of 2–10 minutes. Furthermore, recent spectroscopic studies using the EUV Imaging Spectrometer (EIS) on board *Hinode* have shown that the Doppler shift variations are in phase with the intensity variations (Wang et al. 2009). All of these signatures were shown to be consistent with slow magnetoacoustic waves propagating upward along coronal structures. Slow waves are compressive, essentially longitudinal in a low-β structured plasma (transverse wavelengths much smaller than the longitudinal ones), and propagating at a phase speed near the coronal sound speed (Spruit 1982; Ofman et al. 1999; Nakariakov et al. 2000). The observed propagation speed, which is thus the phase speed projected on the plane of the sky, is always equal or less than the sound speed. Stereoscopic observations of quasi-periodic intensity perturbations, combined with spectroscopy, are indeed in agreement with propagation at the speed of sound, consistent with the temperature of the supporting structure (Marsh et al. 2009). Also, comparison of observations in different temperature bandpasses has shown that the perturbations propagate at different speeds consistent with the change in temperature (Robbrecht et al. 2001; King et al. 2003). The attenuation of the perturbations with height is explained in terms of wave damping by thermal conduction (Nakariakov et al. 2000; De Moortel & Hood 2003; Verwichte et al. 2008).

Recently, observational studies using the X-Ray Telescope (XRT) on board *Hinode* have revealed signatures of quasi-periodic propagating intensity perturbations at the edge of active regions (temperature around 1.1 MK), traveling at speeds of 140 km s^{-1}, and which arguably were interpreted by Sakao et al. (2007) in terms of continuous flows (see also He et al. 2010). Also, a correlation between Doppler shifts and line broadenings as well as significant deviations in the blue wing of line profiles has been found in EIS observations by Hara et al. (2008). Moreover, EIS observations of asymmetries in line profiles, with faint blue-wing excess in the order of 1%–5% core intensity, were used to support the alternative suggestion that the quasi-periodic propagating intensity perturbations could be explained as periodic high-speed (50–100 km s^{-1}) upflows instead of slow waves (De Pontieu et al. 2009; McIntosh & De Pontieu 2009; McIntosh et al. 2010).

Waves and flows are in general of course not mutually exclusive phenomena. Persistent Doppler blue and redshifts have been observed, using EIS, in active region loops, and interpreted as up and down flows with speeds of the order of 20–50 km s^{-1} (e.g., Doschek et al. 2008; Del Zanna 2008), more modest than the above reported speeds. Downflows are stronger in cooler structures while upflows are found in faint, 1.2–1.4 MK hot, long loops.

The study of the spectral signature of slow waves in the solar atmosphere has a long history (e.g., Eriksen & Maltby 1967; McWhirter & Wilson 1974; Byerley et al. 1978; McClements et al. 1991; Hansteen 1993; Brynildsen et al. 2003). Here, we address the specific question whether the new observational spectral signatures seen in events of quasi-periodic intensity perturbations are consistent with a slow wave interpretation. A correct interpretation is of consequence for our understanding of energy transport, dissipation, and wind acceleration in these structures as well as for the seismological exploitation using

[4] Current address: Centrum voor Plasma Astrofysica and Leuven Mathematical Modeling and Computational Science Centre, KU Leuven, Celestijnenlaan 200B, 3001 Heverlee, Belgium.

slow waves (e.g., Robbrecht et al. 2001; King et al. 2003; Wang et al. 2009).

2. SLOW WAVE MODEL

A slow magnetoacoustic wave in a coronal structure of low plasma-β is guided to propagate along the structure parallel to the magnetic field. Hence, the wave is almost completely longitudinal and one dimensional. For simplicity, we model the slow wave as a one-dimensional, small amplitude plane sound wave propagating upward in a static equilibrium plasma that is uniform along the magnetic field. Such a wave is described by the solution (Landau & Lifshitz 1987)

$$v' = a\, c_s \cos(x - c_s t), \quad \frac{1}{(\gamma - 1)}\frac{T'}{T_0} = \frac{n'}{n_0} = \frac{v'}{c_s}, \qquad (1)$$

where $n'(x, t)$, $T'(x, t)$, and $v'(x, t)$ are the wave perturbations in number density, temperature, and velocity, respectively. The quantities with subscript "0" indicate the equivalent constant equilibrium quantities. Also, γ is the ratio of specific heats, c_s is the equilibrium sound speed, and a is the relative wave amplitude, which is assumed to be small, i.e., $a \ll 1$. The wave has a phase $\phi = kx - \omega t$, wavenumber k, and frequency $\omega = c_s k$. Effects of gravitational stratification, dissipation (e.g., thermal conduction), and variations in loop cross section will cause the amplitude a to be a function of height with increasing amplitude due to stratification and decreasing amplitude due to dissipation and cross-section divergence. These phenomena have been studied in the regimes of wavelengths shorter or similar to the typical longitudinal length scales (Nakariakov et al. 2000; Verwichte et al. 2001; De Moortel & Hood 2004).

3. EMISSION LINE MODIFIED BY A SLOW WAVE

The emission of a coronal resonant spectral line from a coronal volume element is modeled as

$$\epsilon(\lambda) \sim n^2 \exp\left[-\frac{(\lambda - \lambda_c)^2}{2(\Delta\lambda)^2}\right]. \qquad (2)$$

The observed intensity is the total emission along the line of sight, i.e., $I(\lambda) = \int \epsilon(\lambda, x) dx$. The quantities λ_c and $\Delta\lambda$ are the line center and width, respectively. For thermal line broadening, the width is of the form $\Delta\lambda = \lambda_c v_{th}/c_0$, where c_0 is the speed of light and v_{th} is the ion thermal speed. We shall illustrate our findings throughout using an emission line from an iron ion minority species at a temperature of 1 MK ($v_{th} = 12$ km s^{-1}, $c_s/v_{th} = 12.5$), which is convolved by the spectral resolution of the EIS instrument. The intensity is furthermore proportional to a function, which contains information about ionization and depends on temperature and (weakly) on density. We shall assume, for the sake of clarity in what follows, that over the range of temperatures that the slow wave covers, this function is constant (see, e.g., De Moortel & Bradshaw 2008 for a study of the effect of ionization on slow wave diagnostics).

The presence of the slow wave in the emitting plasma modifies the strength, center and width of the emission line as a function of space and time as

$$n(x, t) = n_0 \left(1 + \frac{n'}{n_0}\right), \qquad (3)$$

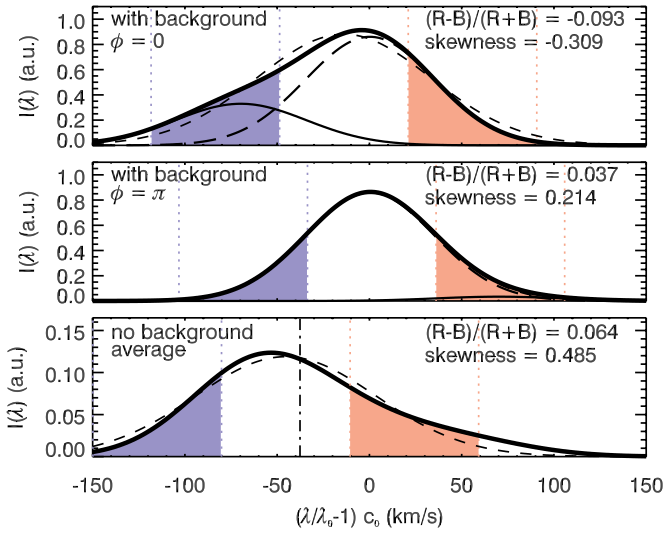

Figure 1. Principles of how a propagating slow wave modifies an emission line are shown. The thick solid curve is the total line emission from a static plasma and a plasma containing a slow wave (shown individually as solid and long-dashed curves, respectively) at oscillation phases $\phi = 0$ (top) and $\phi = \pi$ (middle), which represent upward and downward wave motion, respectively. Also, $ac_s = 70$ km s^{-1}, $\alpha = 0$, and $I_{bg}/I_0 = 2.5$. The dashed line is a Gaussian fit to the line profile. The vertical dotted lines outline the regions between 1 and 3 line widths from the line center. The bottom panel shows the time average emission line with $I_{bg}/I_0 = 0$. The vertical dot-dashed line is the analytical approximated velocity Doppler shift $-\bar{f}_1 \Delta\lambda_0 c_0/\lambda_0$. In each panel, the *R–B* and skewness measures are shown in the top right.

(A color version of this figure is available in the online journal.)

$$\lambda_c(x, t) = \lambda_0 \left(1 - \frac{v' \cos\alpha}{c_0}\right), \qquad (4)$$

$$\Delta\lambda(x, t) = \Delta\lambda_0 \left(1 + \frac{T'}{T_0}\right)^{1/2}. \qquad (5)$$

The Doppler velocity shift involves the line-of-sight velocity component $v' \cos\alpha$, where α is the angle between the direction of propagation and the line of sight. Equations (3)–(5) describe the effects of intensity variations due to the wave density perturbation, Doppler shifts due to the wave velocity field, and thermal line broadening due to the wave temperature perturbation. Because the density and temperature perturbations are in phase with the velocity for a propagating slow wave, the emission from the plasma is enhanced during the upward (blueshift) propagating phase of the wave and is decreased during the downward (redshift) propagating phase of the wave. This inherently asymmetric behavior is illustrated in Figure 1. From Equation (2), it can be seen that the emission line will be a symmetric Gaussian profile at any given time from a single plasma element in which a slow wave is present. In order for the line to be asymmetric either the emission is averaged over a period of oscillation or an additional quasi-static plasma source is taken along the line of sight. The former case is relevant for spectral raster scans where temporal resolution is traded for spatial resolution, while the latter case is relevant for spectral slit measurements.

3.1. Asymmetry of a Time-averaged Line

To understand how an average blue–red wing asymmetry is produced by a slow wave, we expand the line profile (2) relative

to the equilibrium, using $s = (\lambda - \lambda_0)/\Delta\lambda_0$ and $a \ll 1$, to $O(a^2)$ accuracy:

$$\epsilon(s,x,t) \sim n_0^2 \left(1+\frac{n'}{n_0}\right)^2 \exp\left[-\frac{\left(s+\frac{v'\cos\alpha}{v_{\rm th,0}}\right)^2}{2\left(1+\frac{T'}{T_0}\right)}\right],$$
$$\approx n_0^2\left[f_0(x,t)F(s)+\sum_{m=1}^{4}\frac{f_m(x,t)}{m!}\frac{d^mF(s)}{ds^m}\right], \quad (6)$$

with coefficients

$$f_0 = 1+\frac{1}{2}\frac{T'}{T_0}+2\frac{n'}{n_0}+\frac{3}{8}\left(\frac{T'}{T_0}\right)^2+\left(\frac{n'}{n_0}\right)^2+\left(\frac{T'}{T_0}\right)\left(\frac{n'}{n_0}\right),$$
$$f_1 = \left(1+\frac{1}{2}\frac{T'}{T_0}+2\frac{n'}{n_0}\right)\frac{v'\cos\alpha}{v_{\rm th,0}},$$
$$f_2 = \frac{T'}{T_0}+\frac{3}{2}\left(\frac{T'}{T_0}\right)^2+\left(\frac{v'\cos\alpha}{v_{\rm th,0}}\right)^2+2\left(\frac{T'}{T_0}\right)\left(\frac{n'}{n_0}\right),$$
$$f_3 = 3\frac{T'}{T_0}\frac{v'\cos\alpha}{v_{\rm th,0}}, \quad f_4 = 3\left(\frac{T'}{T_0}\right)^2, \quad (7)$$

and $F(s) = \exp(-s^2/2)$. The equilibrium thermal speed is related to the equilibrium line width as $v_{\rm th,0}/c_0 = \Delta\lambda_0/\lambda_0$. Expansion (6) is similar to the Gaussian–Hermite expansion of spectral lines (van der Marel & Franx 1993), which can be seen by identifying $d^mF(s)/ds^m = (-1)^mF(s)H_m(s)$, where $H_m(s)$ is the Hermite polynomial of order m (Abramowitz & Stegun 1965).

Since the perturbations are all proportional to $a\cos\phi$, when averaged over an oscillation period, only the equilibrium and quadratic perturbation terms have non-zero contributions. We denote time-averaged quantities by a bar. The average intensity $\bar{I}(s) = (\omega/2\pi)\int_0^{2\pi/\omega} I(s,t)dt$ may be written with the average emission $\epsilon(s)$ as the sum of a Gaussian profile $F(s_*)$ and third- and fourth-order derivatives of a Gaussian:

$$\bar{\epsilon}(s) \approx n_0^2\left[\left(\bar{f}_0-\frac{\bar{f}_2}{2}\right)F(s_*)+\sum_{m=3}^{4}\frac{\bar{f}_m}{m!}\frac{d^mF(s_*)}{ds^m}\right], \quad (8)$$

where

$$\bar{f}_0-\frac{\bar{f}_2}{2} = 1+\frac{a^2}{16}(8-3(\gamma-1)^2)-\frac{a^2}{4}\left(\frac{c_{\rm s}\cos\alpha}{v_{\rm th,0}}\right)^2,$$
$$\bar{f}_1 = \frac{a^2}{4}(\gamma+3)\frac{c_{\rm s}\cos\alpha}{v_{\rm th,0}},$$
$$\bar{f}_2 = \frac{a^2}{4}(\gamma-1)(3\gamma+1)+\frac{a^2}{2}\left(\frac{c_{\rm s}\cos\alpha}{v_{\rm th,0}}\right)^2,$$
$$\bar{f}_3 = \frac{3a^2}{2}(\gamma-1)\frac{c_{\rm s}\cos\alpha}{v_{\rm th,0}}, \quad \bar{f}_4 = \frac{3a^2}{2}(\gamma-1)^2. \quad (9)$$

The argument of the Gaussian profile is defined as

$$s_* = \frac{s+\bar{f}_1}{\sqrt{1+\bar{f}_2}} = \frac{sv_{\rm th,0}-v_{\rm D}}{\sqrt{v_{\rm th,0}^2+(\Delta v_{\rm NT})^2}}. \quad (10)$$

The line deformations imposed by the slow wave cause, first, a Doppler shift in the line by $v_{\rm D} = -\bar{f}_1 v_{\rm th,0}$ to the blue wing; second a non-thermal line broadening $\Delta v_{\rm NT} = \bar{f}_2^{1/2} v_{\rm th,0}$; and, third, an asymmetry through the term involving the third derivative of F. Using Equation (9), it can be seen that for a heavy ion with $c_{\rm s} \gg v_{\rm th,0}$, the non-thermal line broadening is approximately equal to $\Delta v_{\rm NT} \approx ac_{\rm s}\cos\alpha/\sqrt{2}$. Therefore, mainly through its velocity perturbation, the slow wave produces a line broadening that is proportional to the wave amplitude. The Doppler velocity and line broadening are strongly correlated. For instance, a Doppler velocity of 5 km s^{-1} has an associated non-thermal line width of approximately 20 km s^{-1}, consistent with observations reported by Hara et al. (2008). Furthermore, for an iron emission line, using Equation (9), $\bar{f}_3 \approx 10a^2$. Therefore, a slow wave with a relative amplitude of 5% is likely to produce an average line asymmetry of the order of a few percent. Figure 2 shows the Doppler shift, line broadening, and line asymmetry as a function of a using Equations (2)–(5). Figure 2 shows that $v_{\rm D}$ and $\Delta v_{\rm NT}$ follow the analytical approximations in the range of observed amplitudes.

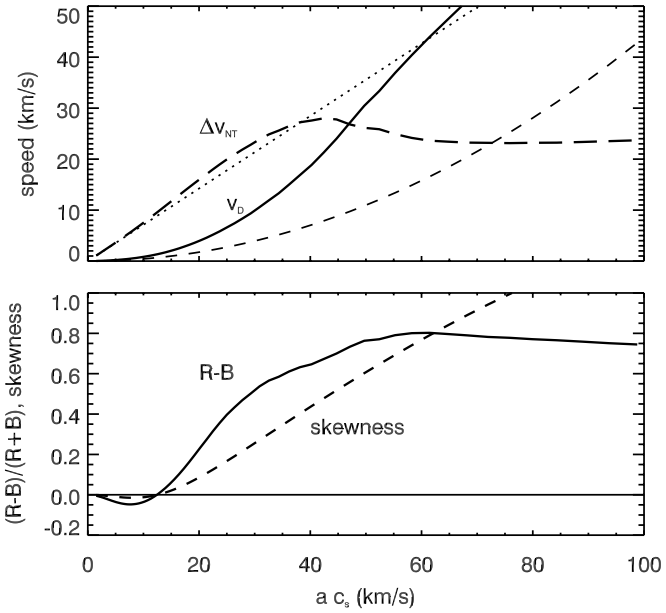

Figure 2. Top: velocity Doppler shift (solid) and non-thermal line width speed (long-dashed) as a function of wave amplitude $ac_{\rm s}$. The dotted and dashed line is the analytical approximation based on Equation (8). Bottom: R–B (solid) and skewness measures (dashed) as a function of wave amplitude $ac_{\rm s}$.

The line asymmetry is characterized using quantities B and R, which are the integrated intensity between 1 and 3 line widths from the line center in the red and blue wings of the line, respectively. Hence, $(R-B)/(R+B)$ gives a measure of the asymmetry in the wings of the line profile with negative values representing an excess in the blue wing (De Pontieu et al. 2009). An alternative measure of line asymmetry is skewness, defined as $\int((s-s_0)/\sigma)^3 I(s)ds/\int I(s)ds$, where s_0 and σ are the mean and standard deviation of the line. It is consistent with the R–B measure in showing a bias toward the blue wing for small amplitudes and red wing bias for large amplitudes where the average line forms a heavier red wing. Figure 2 shows that both measures show similarly a growing blue-wing bias as a function of wave amplitude.

3.2. Asymmetry of a Multi-component Line

First, we consider the profile of an emission line which constitutes emission from two plasma components in the line of sight:

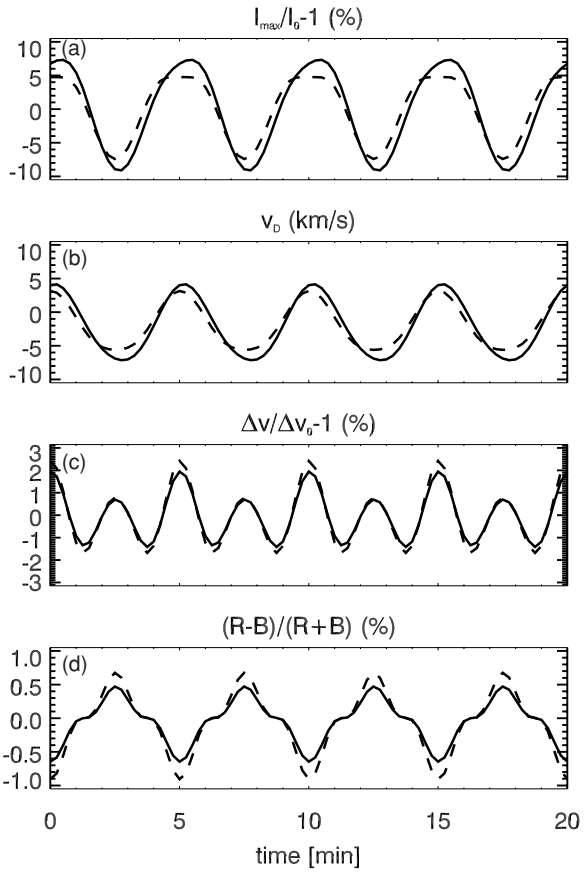

Figure 3. Relative spectral line signatures as a function of time for an emission line obtained using Equations (2)–(5): (a) relative peak intensity variation $\max(I)/\max(I_0) - 1$, (b) Doppler shift, v_D, (c) relative line width variation, $\Delta v/\Delta v_0$, and (d) relative left–right wing asymmetry. The dashed curves represent the superposition of a plasma with a slow wave of velocity amplitude $0.15c_s$ and a period of 5 minutes and a static plasma, which contributes 2/3 of the total integrated emission. The solid curves represent the integrated emission line along the loop over a distance of 10 Mm where the wave amplitude is of the form $a(x) = C - D\tanh((x - x_0)/\Delta x))$ where the value of the constants is as explained in the main text.

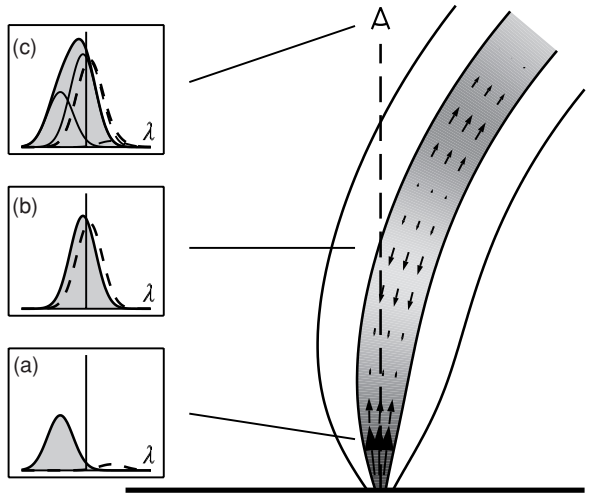

Figure 4. Illustration of the formation of an emission line signature from line-of-sight integration across a loop with a propagating slow wave, whose amplitude may vary with distance from the footpoint, and a static background plasma. The velocity field and intensity perturbation of the slow wave are shown. The inset figures illustrate the emission line at various locations. The solid and dashed curves are for oscillation phase $\phi = 0$ and $\phi = \pi$, respectively. (a) Emission line from the loop with a large amplitude slow wave. (b) Emission line from loop with small amplitude slow wave or from a static background plasma in the line of sight. (c) Total emission line integrated over the line of sight. The thin lines show the two plasma components contributing to the full profile.

(1) a quasi-static "background" and (2) the plasma structure supporting a propagating slow wave. The "background" plasma refers here to another plasma in the same line of sight distinct from the "background equilibrium" plasma structure through which the slow wave is propagating. This is modeled for small amplitudes using Equation (6) by replacing the term of $O(1)$ in f_0 by $1 + I_{bg}/I_0$, where I_{bg} is the background and I_0 is the structure's equilibrium plasma emission. Figure 1 illustrates that for two oscillation phases, $\phi = 0, \pi$, the effect of the slow wave on the combined line is variations in intensity, Doppler shift, line width, and line asymmetry, the strength of which depends on I_{bg}/I_0. The intensity and Doppler velocity variations are reduced by a factor $1/(1 + I_{bg}/I_0)$. Therefore, even though the slow wave may have a large amplitude, the resulting intensity and Doppler velocity may be small. Again, the contributions of order $O(a^2)$ in Equation (6) introduce stronger emission in the blue wing. Figure 3 shows an example of the simulated spectral line signatures from a single Gaussian fit to the line as a function of time for a slow wave with a period of 5 minutes and $a = 0.15$, and a static plasma component with $I_{bg} = 2I_0$. Oscillations of reduced amplitude are seen in the intensity and Doppler velocity. Also, the line width has the tendency to show a half-period oscillation with an amplitude of approximately 1 km s^{-1} and is caused by an excursion of the wave contributed line toward both blue and red wing of the static line. The spectral signatures are consistent with recent observations by De Pontieu & McIntosh (2010), except for the half-period oscillation in the line width. However, the addition of a modest steady upflow as reported could diminish the excursions into the red wing of the static line and cause the line width to oscillate with the same period. Importantly, an oscillation in the line asymmetry with a maximum value up to 1% is seen (the skewness shows the same time profile).

A quasi-static plasma is needed in the line of sight to produce a periodic line asymmetry but it does not necessarily have to be separate from the oscillating structure. Because periodic line asymmetries have been reported at or near the footpoints of the loops, we may be observing the integrated intensity along an extended section of the loop. During the wave's propagation its amplitude is affected by dissipation and variations in loop cross section, which decrease the amplitude, and gravitational stratification, which enhances it (Nakariakov et al. 2000). Also, fluctuations in the driver may cause the wave amplitude to vary with time (and distance). Hence, when integrating along a section of the loop, we have the superposition of different wave amplitudes. This scenario has been illustrated in Figure 4. Consider as an illustration the case where the wave field rapidly decreases with height due to a rapid expansion of the loop cross section or dissipation. As an example, we consider a profile $a(x) = C - D\tanh((x - x_0)/\Delta x))$ with $x_0 = 2$ Mm and $\Delta x = 0.5$ Mm, and where constants C and D are chosen such that $a(0) = 0.15$ and $a(10\text{ Mm}) = 0.01$, respectively. This profile essentially superimposes a small contribution of a large amplitude slow wave on a large contribution of a small amplitude wave. Figure 3 shows the associate spectral signatures, which are essentially the same as the case with a static background. This includes the presence of excess in the blue wing of the line. The departure from sinusoidal profiles in the intensity and Doppler velocity time series is due to the integration over

a distance of approximately 20% of the wave length. Such a model also explains the observed spectral signatures at greater heights (Wang et al. 2009). The amplitude profile used here is not unique. In fact, it may be increasing with height first due to density stratification before decreasing (Nakariakov et al. 2000). Provided large and small wave amplitudes are superimposed in the line of sight, similar line asymmetries are expected.

4. CONCLUSIONS

Propagating slow waves can naturally explain observed coronal spectral signatures of in-phase Doppler velocity and intensity of the observed quasi-periodic perturbations (Wang et al. 2009). Also, a slow wave, when averaged over its period of oscillation, produces non-thermal line broadening that is correlated with the Doppler velocity as found in observations reported by Hara et al. (2008). The additional signature of line asymmetry is explained qualitatively by including a quasi-static plasma component in the line of sight, which may originate from a separate background plasma or from an extended part of the structure in which the wave propagates. Importantly, contrary to the alternative periodic upflow theory, the slow wave will continue to show signatures of oscillations in Doppler velocity even without the static component. We have modeled the line asymmetry using a single Gaussian spectral fit and with the $R-B$ measure employed by De Pontieu et al. (2009). However, a detailed analysis would require multi-component spectral fits (Peter 2010). We note that a small $O(a^2)$ correction term may be added to the wave velocity to ensure that there is no net mass flux (Byerley et al. 1978). However, this does not substantially change the results.

We conclude that slow magnetoacoustic waves remain a valid explanation for the observed quasi-periodic intensity perturbations. Many questions still remain about their origin at the loop footpoint, i.e., the excitation mechanism, the role of strong longitudinal structuring and background flows. Future combined imaging and spectral observations using the Atmospheric Imaging Assembly on the Solar Dynamics Observatory and EIS/*Hinode* observations will undoubtedly provide more insight. The quantitative prediction of spectral slow wave signatures to compare with observations is the subject of a future work. This requires detailed spectral information (e.g., Dere et al. 1997), a realistic loop atmosphere model, and the calculation of the associated slow wave solution with height (building on, e.g., Hansteen 1993; Nakariakov et al. 2004).

E.V. acknowledges financial support from the UK Engineering and Physical Sciences Research Council (EPSRC) Science and Innovation award. M.M. is supported by the UK Science and Technology Facilities Council (STFC) under grant number ST/F002769/1. C.F. acknowledges financial support from STFC on the CFSA Rolling Grant. T.V.D. acknowledges the support from the Marie Curie Intra-European Fellowship within the 7th European Community Framework Programme under grant agreement no. 220555. I.D.M. acknowledges support from a Royal Society University Research Fellowship.

REFERENCES

Abramowitz, M., & Stegun, I. A. 1965, Handbook of Mathematical Functions: with Formulas, Graphs, and Mathematical Tables (New York: Dover)
Berghmans, D., & Clette, F. 1999, Sol. Phys., 186, 207
Brynildsen, N., Maltby, P. O., Kjeldseth-Moe, O., & Wilhelm, K. 2003, A&A, 398, L15
Byerley, A., McWirter, R. W. P., & Wilson, R. 1978, J. Phys. B: Atom. Mol. Phys., 11, 613
DeForest, C. E., & Gurman, J. B. 1998, ApJ, 501, L217
Del Zanna, G. 2008, A&A, 481, L49
De Moortel, I. 2009, Space Sci. Rev., 149, 65
De Moortel, I., & Bradshaw, S. J. 2008, Sol. Phys., 252, 101
De Moortel, I., & Hood, A. W. 2003, A&A, 408, 755
De Moortel, I., & Hood, A. W. 2004, A&A, 415, 705
De Moortel, I., Hood, A. W., Ireland, J., & Walsh, R. W. 2002, Sol. Phys., 209, 61
De Moortel, I., Ireland, J., & Walsh, R. W. 2000, A&A, 355, L23
De Pontieu, B., & McIntosh, S. W. 2010, ApJ, 722, 1013
De Pontieu, B., McIntosh, S. W., Hansteen, V. H., & Schrijver, C. J. 2009, ApJ, 701, L1
Dere, K. P., Landi, E., Mason, H. E., Monsignori Fossi, B. C., & Young, P. R. 1997, A&AS, 125, 149
Doschek, G. A., Warren, H. P., Mariska, J. T., Muglach, K., Culhane, J. L., Hara, H., & Watanabe, T. 2008, ApJ, 686, 1362
Eriksen, G., & Maltby, P. 1967, ApJ, 148, 833
Hansteen, V. 1993, ApJ, 402, 741
Hara, H., Watanabe, T., Harra, L. K., & Culhane, J. L. 2008, ApJ, 678, L67
He, J.-S., Marsch, E., Tu, C.-Y., Guo, L.-J., & Tian, H. 2010, A&A, 516, A14
King, D. B., Nakariakov, V. M., Deluca, E. E., Golub, L., & McClements, K. G. 2003, A&A, 404, L1
Landau, L. D., & Lifshitz, E. M. 1987, Fluid Mechanics (2nd ed.; Oxford: Pergamon)
Marsh, M. S., Walsh, R. W., De Moortel, I., & Ireland, J. 2003, A&A, 404, L37
Marsh, M. S., Walsh, R. W., & Plunkett, S. 2009, ApJ, 697, 1674
McClements, K. G., Harrison, R. A., & Alexander, D. 1991, Sol. Phys., 131, 41
McEwan, M. P., & De Moortel, I. 2006, A&A, 448, 763
McIntosh, S. W., & De Pontieu, B. 2009, ApJ, 706, L80
McIntosh, S. W., Innes, D. E., De Pontieu, B., & Leamon, R. J. 2010, A&A, 510, L2
McWhirter, R. W. P., & Wilson, R. 1974, J. Phys. B: Atom. Mol. Phys., 7, 1588
Nakariakov, V. M., Tsiklauri, D., Kelly, A., Arber, T. D., & Aschwanden, M. J. 2004, A&A, 414, L25
Nakariakov, V. M., Verwichte, E., Berghmans, D., & Robbrecht, E. 2000, A&A, 362, 1151
Ofman, L., Nakariakov, V. M., & Deforest, C. E. 1999, ApJ, 514, 441
Ofman, L., Romoli, M., Poletto, G., Noci, C., & Kohl, J. L. 1997, ApJ, 491, L111
Peter, H. 2010, A&A, in press
Robbrecht, E., Verwichte, E., Berghmans, D., Hochedez, J.-F., Poedts, S., & Nakariakov, V. M. 2001, A&A, 370, 591
Sakao, T., et al. 2007, Science, 318, 5856
Schrijver, C. J., et al. 1999, Sol. Phys., 187, 261
Spruit, H. C. 1982, Sol. Phys., 75, 3
van der Marel, R. P., & Franx, M. 1993, ApJ, 407, 525
Verwichte, E., Haynes, M., Arber, T. D., & Brady, C. S. 2008, ApJ, 685, 1286
Verwichte, E., Nakariakov, V. M., Berghmans, D., & Hochedez, J.-F. 2001, in ESA-SP, 493, Solar Encounter. Proc. of the First Solar Orbiter Workshop, ed. B. Battrick & H. Sawaya-Lacoste (Noordwijk: ESA), 39
Wang, T. J., Ofman, L., & Davila, J. M. 2009, A&A, 503, L25